33RD CONGRESS
OF THE INTERNATIONAL COUNCIL
OF THE AERONAUTICAL SCIENCES
STOCKHOLM, SWEDEN, 4-9 SEPTEMBER, 2022

ICAS 2022 SWEDEN

EXPERIMENTAL EVALUATION OF A PASSIVE FLOW-CONTROL DEVICE FOR A TILTROTOR AIRCRAFT

Anderson R. Proença[1], Simon A. Prince[1], Lynton Banks-Davies[1] & Kevin P. Garry[1]

[1]School of Aerospace, Transport and Manufacturing, Cranfield University, Cranfield, MK43 0AL, UK

Abstract

This work presents a preliminary investigation into tiltrotor propeller/nacelle/wing flows, and the flow breakdowns that can lead to the phenomenon of whirl flutter. Static blade measurements were performed, results suggesting that tubercles have the potential to provide an increase in performance for the baseline blade design. A small-scale propeller rig (0.7 m swept diameter) has been designed, manufactured, and commissioned at Cranfield's 8x6 Wind Tunnel. This new rig operates well under static and up to wind speeds of at least 30 m/s. The effect of blade pitch angle (0 to 10°) and propeller rotational speed (0 to 3000 rpm) have been investigated successfully. Forces measured on the wing set at angles of attack within the range 0 to 22° indicate the well-established effects due to propeller slipstream. Overall, the propeller wake flow slightly decreases the lift generated by the wing model, whilst also delaying stall. Pressure taps and accelerometers mounted on the wing and propeller nacelle effectively captured the slipstream effects, blade passing frequency, and flow separation regions. Finally, blades containing tubercle-shaped vortex generators were mounted to the propeller rig. Preliminary test results for the tubercle blades are reported in the paper. Overall, effects due to the propeller slipstream are dominant on forces, pressure distribution and vibration of the wing model. At the current stage of this ongoing investigation, it is not possible to conclude whether the tubercles provide any benefit to either the propeller or wing aerodynamic efficiencies. The rig is being equipped to measure propeller thrust and torque. Flow field investigation will also be carried out in future campaigns.

Keywords: tiltrotor; vortex generators; propeller; pressure distribution; wind tunnel measurements

1. Introduction

Tiltrotor aircraft have had intermittent bursts of interest and development [1]. Combining advantages observed in helicopters and fixed-wing aircraft, tiltrotor vehicles are seen to be a sought-after alternative to novel Urban Air Mobility (UAM) vehicles. Additionally, the success of well-known aircraft such as the Bell-Boeing V-22 Osprey has contributed to a strong renewed enthusiasm towards tiltrotors aiming at performing vertical takeoff and landing (VTOL) and short takeoff and landing (STOL) maneuvers.

The UK Vertical Lift Network (UK VLN) has been working on the development of tools to design the next generation of these tiltrotors and other rotorcraft. A significant part of the UKVLN activities stem from the EPSRC funded project entitled 'Methods and Experiments for NOvel Rotorcraft' (MENtOR). One adverse phenomenon associated with tiltrotors, where the mass of the engine/propeller is located on the end of a non-rigid wing, is whirl flutter. This potentially devastating effect is stimulated by both the periodic forcing from both gyroscopic and asymmetric aerodynamic forces. The aerodynamic forces result from boundary layer separations from the propeller blades, nacelles, and the wings.

In one of the various work packages of MENtOR a low-speed propeller test rig has been developed at Cranfield University. The rig was designed to test the performance of passive flow control devices both on the suppression of flow breakdown on the propeller blades and on the delay of wing stall flutter. Studying the propeller wake flow interaction with nacelle surfaces is also envisaged in this new

setup. The commissioning of this rig and the preliminary evaluation of vortex generators mounted on the propeller blades are the main subjects discussed in the paper. A secondary aim is to, long term, provide high-quality steady and unsteady aerodynamic data to the scientific community interested in conducting numerical or similar experimental analysis on installed propellers.

The aerodynamic interaction of propellers and wings has been surveyed by several authors [2, 3, 4, 5, 6, 8, 7]. Depending on the direction of rotation, a performance benefit is observed due to the propeller wake flow favourable interaction with the upper and lower surfaces of the wing. The aerodynamics of installed propellers depends strongly on the velocities involved (i.e., propeller angular velocity and wind speed), the angle between the propeller axis and the wing chord, and propeller geometry (i.e., number of blades, blade pitch angle, blade shape).

To inform the design of the propeller experiments and to investigate passive flow control to suppress blade separations in representative flows, static blade tests were conducted using flow visualization technique and force measurements. The blade, mounted on a force balance on an assembly allowing both pitch and sweep, allowed for testing with representative spanwise flows. These tests indicated that 'tubercles' (or 'denticles') mounted along the blade leading edge improve the aerodynamic performance of the blade at several sweep angles and Reynolds numbers. A summary of these results is presented in the paper. Numerical results have been presented in the literature [10, 9, 11], although experimental evidence of the performance of these vortex generators is not yet sufficient. The main objective here is to demonstrate an arrangement of a passive flow control method that can effectively suppress flow separations on the blades, nacelle, and wing, avoiding then any cause of whirl flutter instabilities.

This paper is organized as follows. Key information of the experiments conducted is presented in the next section. In Section 3, results of the static blade experiment are presented. Both surface oil flow visualisation and force measurements are discussed. Then, in Section 4, the propeller rig commissioning is presented. Aerodynamic forces, pressure distribution, and vibration analysis on the wing based on a range of propeller rotational speed and wind speed are investigated. Finally, preliminary investigation of the effects of tubercles arrangement on the wing properties is presented in Section 5, followed by the main conclusions (Section 6).

2. Experimental Methodology

2.1 Experimental Facility and Hardware

Experiments were performed in the Applied Aerodynamics Lab (AAL) at Cranfield University. The static blade test was conducted in the Weybridge open-jet wind tunnel. The propeller rig was tested in the 8x6 Wind Tunnel. Facilities, models, and instrumentation used in the experiments are described below.

2.1.1 Wind tunnel facilities

Static blade tests have been conducted in the Weybridge open-jet wind tunnel. The Weybridge is a subsonic, closed-return wind tunnel, powered by a 40 hp electric motor. The wind speed obtained is stable in the range $10 \leq U_\infty \leq 40$ m/s. The nozzle upstream the working section has an exit diameter of 1.067 m. To enable flow speed monitoring in the working section from static pressure variations along the contraction, both the settling chamber and the nozzle are equipped with one ring of pressure taps each. An image of the Weybridge wind tunnel is illustrated in Fig. 1.

The final propeller tests have been conducted in the 8x6 low-speed wind tunnel, which is part of the EPSRC National Wind Tunnel Facilities (NWTF). This is a closed loop, closed working section wind tunnel, powered by a 550 hp electric motor. The test section has dimensions of 2.4-m wide by 1.8-m high (8 ft by 6 ft), and 5.18-m long. Operation in the 8x6 wind tunnel is stable within the range $10 \leq U_\infty \leq 45$ m/s. Although a two-stage suction system exists in the tunnel for optimisation of the ground plane boundary layer, this has not been utilised, as only measurements on the wing model were studied in the present work.

2.1.2 Static blade and propeller models

For tests performed in the Weybridge, a single blade was manufactured and mounted to a six degree-of-freedom force-torque JR3 load cell. Figure 2 displays the blade and support mounting system used

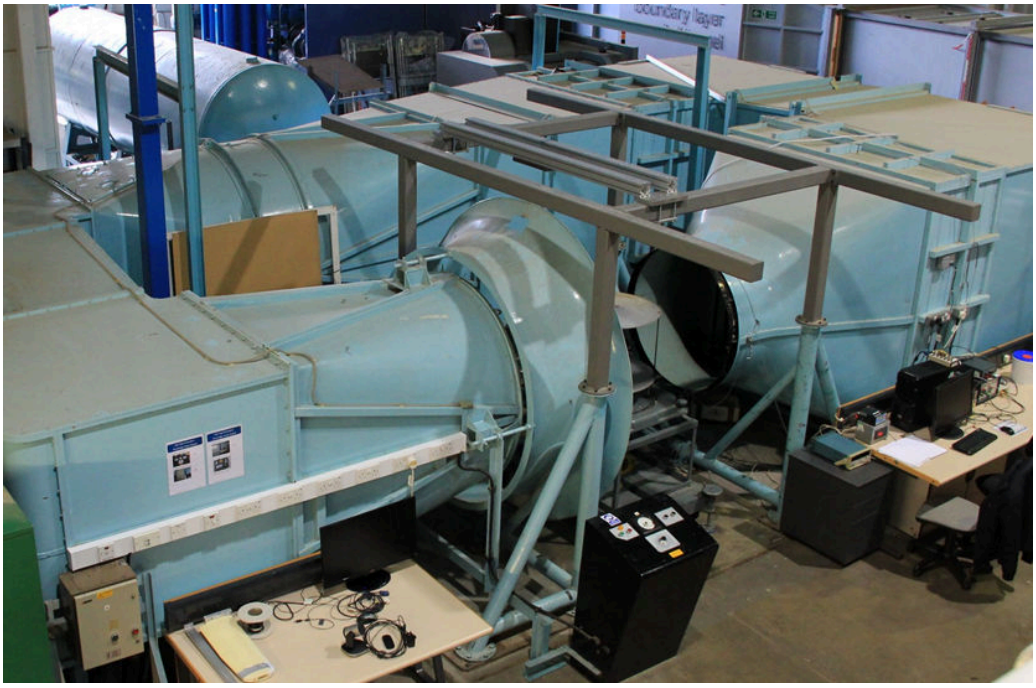

Figure 1 – Image of the Weybridge open-jet wind tunnel.

in the tests. The span of the blade is 445 mm, whilst the root chord length, middle chord length, and tip chord length are 84 mm, 72 mm, and 60 mm, respectively.

Figure 2 – Image displaying the blade model used in the static blade tests and the pivoting system used to set sweep and incidence angles.

A pivoting support structure has been designed and built, allowing the blade to pitch and yaw. This mechanism was used to set the blade at several angles of attack (i.e., from 0 to $16°$, at $4°$ intervals) and sweep angles (i.e., $0°$, $15°$, and $30°$).
The tubercles mounted along the blade leading edge are of three sizes (i.e., diameter of 15 mm close to the root, 8 mm in the middle, and 5 mm close to the tip). Spacing between each tubercle is 20 mm. The blade manufactured for the static blade experiments has the same geometry as the blades

mounted on the propeller rig (scale 1.5:1). The distancing and size of tubercles designed for the propeller rig are, therefore, also scaled down from the static blade tests.
A propeller rig has been designed and manufactured. The propeller has a swept diameter of 0.7 m. These three blades were scaled to 70% of a large-scale model intended to be tested in larger scale experiments to be performed at the University of Glasgow on the UK rotor testing rig. The Cranfield rig is, therefore, a relatively cheaper experimental facility to gain experience and understanding of the various passive flow control strategies for the alleviation of whirl flutter, before implementation on expensive large scale rotor test rigs. Images of the propeller rig and the 8x6 Wind Tunnel test section are displayed in Fig. 3.

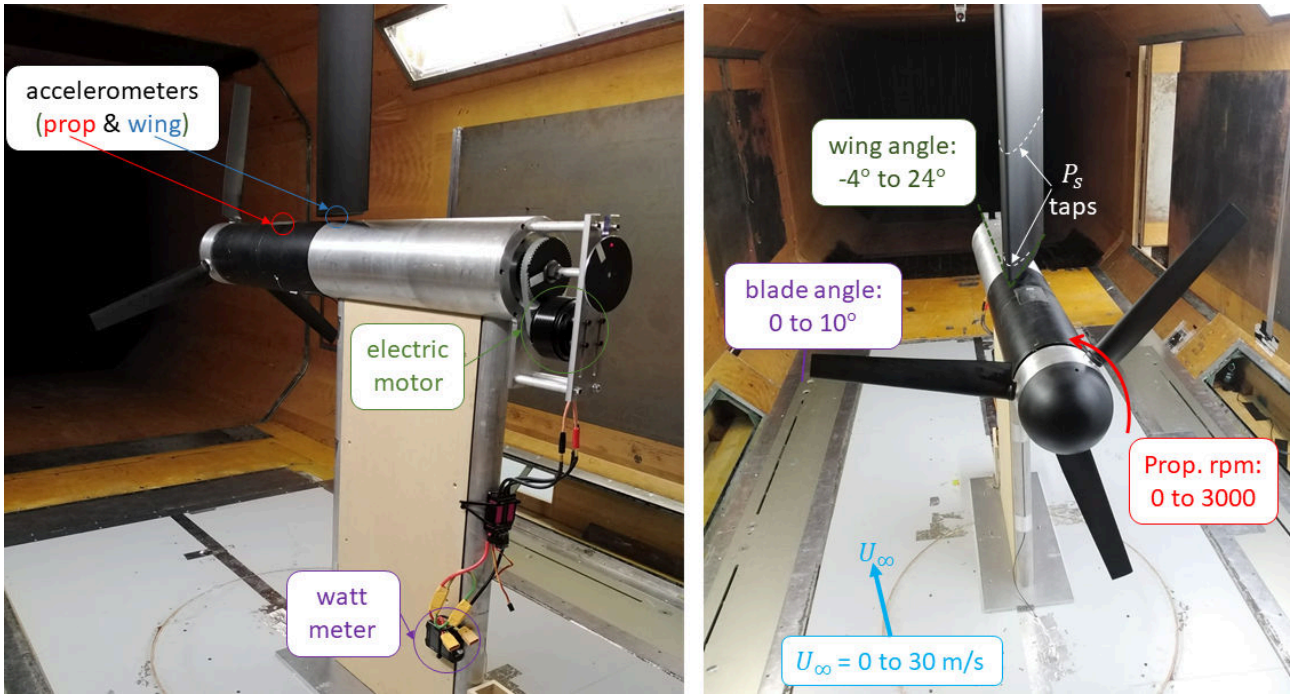

Figure 3 – New propeller test rig with tilting wing in the Cranfield University 8x6 Wind Tunnel.

The propeller shaft is driven by a Dualsky GA 6000 electric motor, which delivers a maximum output of 6.8 kW. A 130 amps electronic speed control (ESC) was coupled to the electric motor and a watt meter was connected between the ESC and the battery pack. Two sets of gearboxes were used in the experiments.
The propeller blades were made of aluminium grade 6082T6. Blades were manufactured using CNC machining. The three blades were mounted in the hub using a mechanism that allows the blade pitch angle to be smoothly varied and set.
Finally, to test the passive flow control devices, new blades have been manufactured. Figure 4 displays a schematic of the geometry used to manufacture the propeller blades, and an image of one of the blades displaying the location and size of the different vortex generators used in the work.

2.1.3 Wing model

The wing model is a rectangular, unswept wing with a NACA 65(2)-415 a=0.6 profile. This profile has been selected to be representative of a modern tiltrotor (i.e., the V-22 Osprey). The main wing dimensions are 0.86-m span and 0.4-m chord. The model was mounted to an overhead balance. The overhead balance is supported by a turntable, which was used to set the wing angle of attack.
The wing has been instrumented with static pressure taps along the mid-cross-section and close to wing tip near the propeller (see Fig. 3). The location of the pressure taps with respect to the wing leading edge are indicated in Fig. 5. Red circles represent sensors in the mid-section (at a spanwise location close to the expected tip vortex impingement), whilst blue crosses indicate pressure taps close to the wing tip (within the quarter-chord only).
In the next section, more details about the instruments used to record data are given.

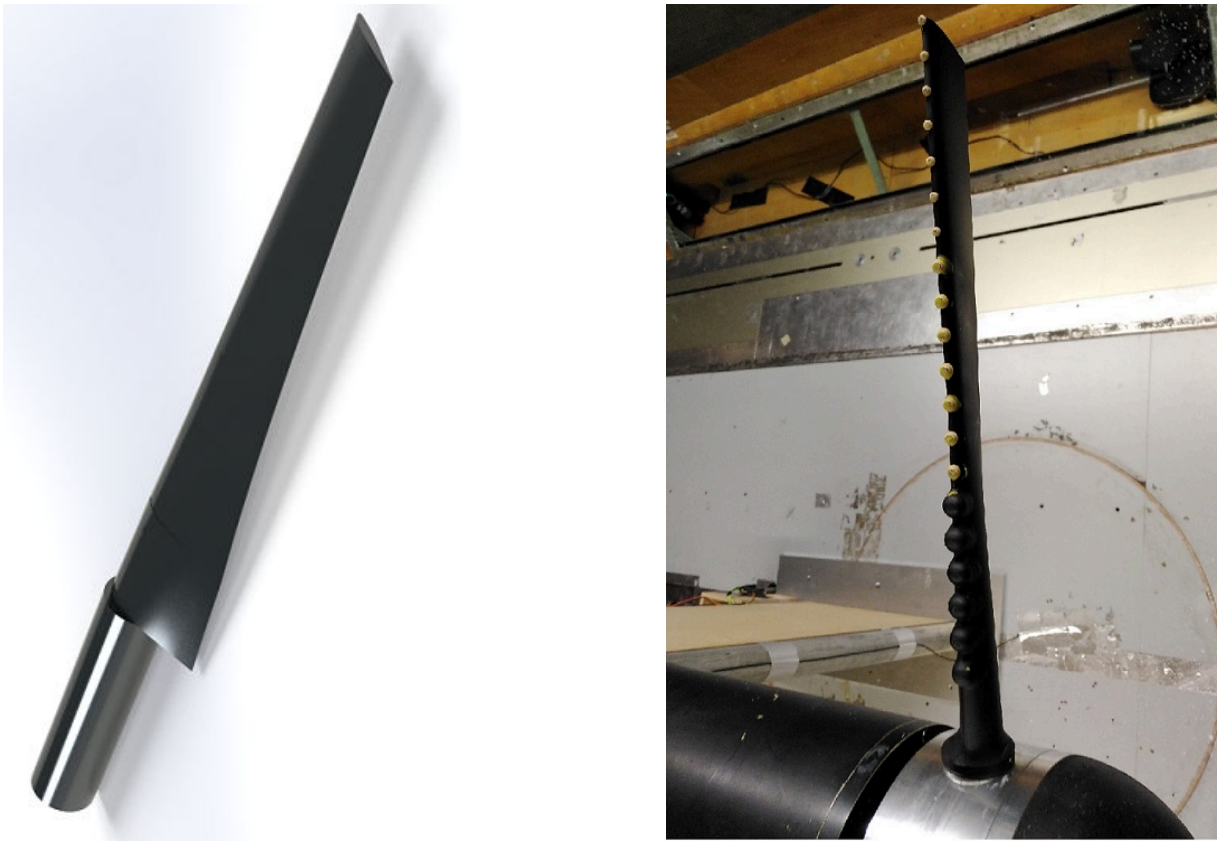

(a) (b)

Figure 4 – Schematics illustrating the blade model and image displaying the 'tubercles' arrangement tested in the work

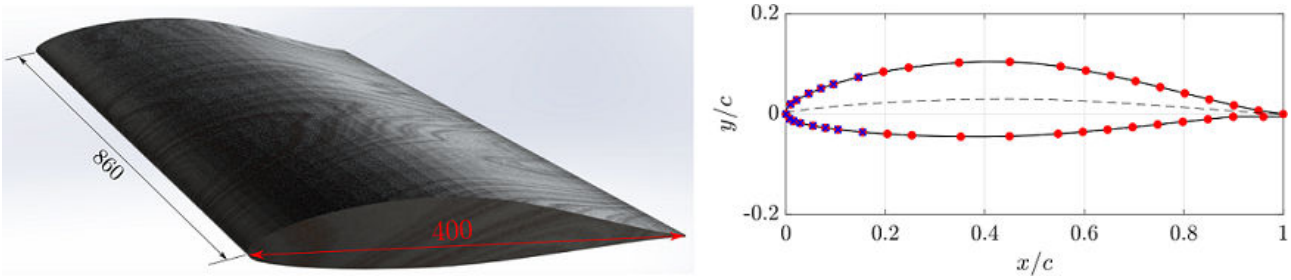

Figure 5 – Illustration of the wing model used and location of the static pressure taps.

2.2 Instrumentation

The wing model was equipped with static pressure taps, one accelerometer, and mounted to an overhead balance. An additional accelerometer was also mounted to the propeller casing. Information about these sensors is provided in the following sub-sections.

2.2.1 Overhead balance

Forces and moments on the wing were measured using an AEROTECH 6-component overhead balance. The three forces obtained are either parallel (i.e., axial force) or perpendicular (i.e., normal and side forces) to the propeller axis and wind speed. Corrections have been applied to the raw data to obtain lift force, drag force, and pitching moment in the analysis presented in the result sections. The overhead balance operates using a dedicated software. Only averaged forces and moments have been recorded. Each of the three orthogonal axes support a maximum applied force which is at least one order of magnitude higher than the forces involved in the experiments.

2.2.2 Static pressure taps

As mentioned in Section 2.1.3pressure taps were distributed in two cross-sections (also illustrated in figures 3 and 5). Near the mid-plane of the wing (i.e., 0.50 m above the propeller axis), 41 pressure taps were mounted. Just 0.15 m above the propeller axis, 15 pressure taps were distributed within the quarter-chord.
The small-bore tubes machined perpendicularly into the wing surface were connected to digital pressure transducer systems by flexible pneumatic tubing. The Cranfield Digital Simultaneous Pressure Scanning System employs differential pressure transducers HCLA0075DB (0 to ± 75 mbar range) manufactured by First Sensor. Only average static pressure data was obtained from the current sensor arrangement.

2.2.3 Accelerometers

Two B&K DeltaTron Piezoelectric Accelerometer Type 4507 have been used in the tests. The location of these on the wing and nacelle are indicated in Fig. 3. These sensors are used to attempt to capture the vibration induced by flow separation on the blades, nacelles, and wing. Obviously, the accelerometer on the propeller also suffers from the vibration created by the motor. Tests with and without the blades were conducted to quantify the motor interference in these measurements. Motor and shaft vibrations are one of the reasons for the gap between the wing and the propeller case.
For the commissioning and preliminary tubercles assessment tests, no attempt at modifying the eigenfrequency of wing and propeller rig has been conducted. An additional tap test has been performed to evaluate the eigenfrequency of the wing model and propeller rig and to verify the sensitivity of the accelerometers. This test has confirmed the non-aerodynamic dominant frequencies associated with each model discussed in the result sections.

2.3 Data Handling

Two data acquisition systems have been used in the experiments. A dedicated software acquires the six-component forces and moments from the overhead balance. The data for each run is recorded as a ten-second average. All data is corrected for the tare measurements performed before each test.
An NI data acquisition DAQ system is used to acquire the static pressure and acceleration data. Only an averaged signal, once more over a ten-second period, is recorded for the pressure taps. Resulting vectors containing the data for all pressure taps are recorded as a matrix. A separate file outputs the time series for acceleration, propeller rpm, and tunnel wind-speed. For the unsteady properties, data is acquired for ten seconds at a sampling rate of 10.24 kilo samples per second.
Data has been post-processed using Matlab scripts and LabView virtual instruments. The frequency-domain analysis of the acceleration signal is conducted by using the averaged periodogram's method (Welch's method). In order to capture the correct nature of the tonal components of each run, the frequency bandwidth has been set to 1 Hz in this investigation. Data is divided into segments with 50% overlap, and a Hann window is applied to each segment before the PSD is taken.

2.4 Nominal Test Matrix

In the static blade tests, the investigation was carried out over a range of blade pitch angles, sweep angles, and wind speeds. For force measurements, five pitch angles were studied, 0° to 16°, at 4° intervals. Three sweep angles (0°, 15°, and 30°) and four wind speeds (18, 28, 32, 36) were tested. Flow visualization tests were performed at angles of attack 0° and 16°, sweep angles 0° and 30°, and the same four speeds as the force experiments.
For the final campaign, the variables investigated in both the rig commissioning and tubercles assessment tests are 1) propeller rotational speed, 2) propeller blade pitch angle, 3) wind speed, and 4) wing angle.
The propeller rotational speed as set from 0 to 3000 revolutions per minute, at 750 rpm intervals. Three blade pitch angles were studied, namely, 0°, 5°, and 10°. A total of four wind speeds (0 to 30 m/s, at 10 m/s intervals) and several wing angles of attack ranging from 0° to 22° were also interrogated.
Finally, some test runs envisaged in the above uniform test matrix were not performed. For example, at wind speed 30 m/s and propeller blade angles 5° and 10°, the propeller rig rotational speed would be around or higher than 3000 rpm (windmill mode). On the contrary, for static tests (i.e., $U_\infty = 0$),

blade pitch angle $10°$, it was not possible to achieve 3000 rpm as the power providing the necessary torque to the propeller rig was higher than the maximum power output of the ESC. Nonetheless, most of the parameters described in the previous paragraph were tested successfully.

3. Results of the Static Blade Test

In this section, key results from the surface flow visualization and force experiments performed in the Weybridge wind tunnel for the static blade are discussed.

3.1 Surface flow visualization

Surface oil flow visualization tests were conducted for a range of Reynolds numbers, blade pitch, and sweep angles. These variables were studied extensively to capture the detailed flow separations, ensuring that spanwise effects were captured. Figure 6 shows a sample ultraviolet illumination oil flow pattern that this technique can provide.

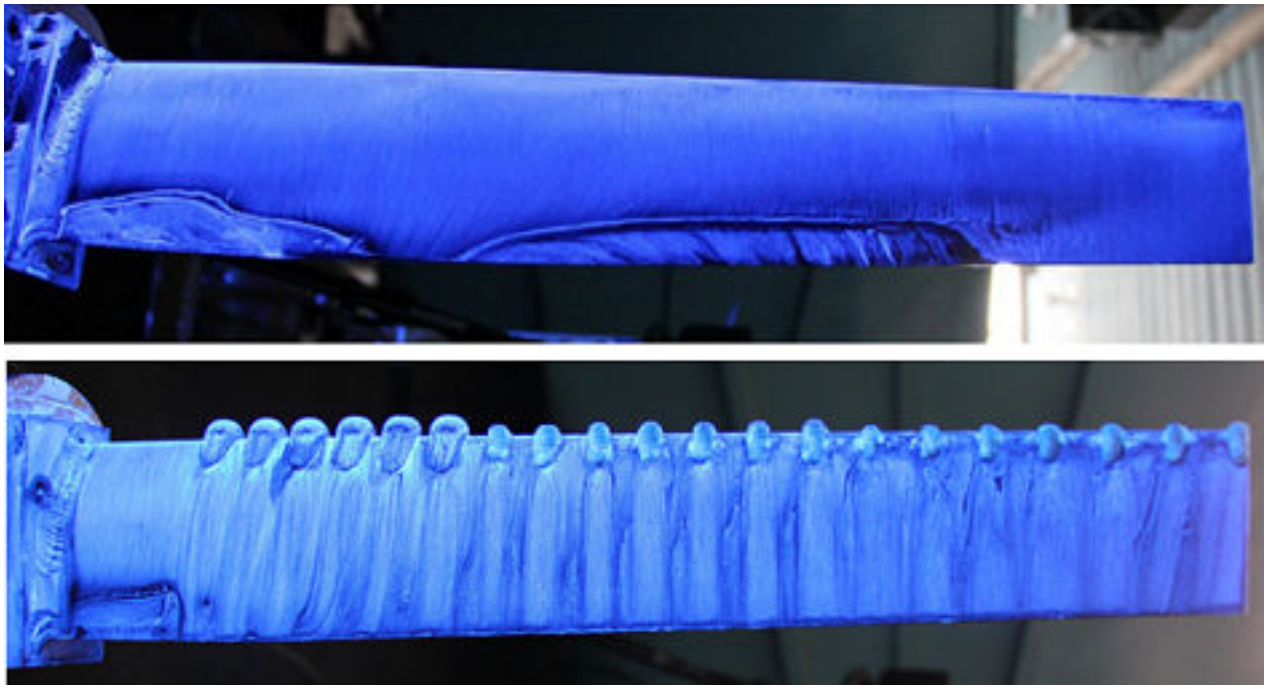

Figure 6 – Upper surface oil flow pattern for the zero blade pitch case at zero sweep at a Reynolds number of 0.144 million based on root chord. Top: clean blade. Bottom: blade with tubercles

It can be seen from Fig. 6 that two recirculation bubbles form near the trailing edge of the clean blade. The tubercles that were added to the blade leading edge, with different geometric configurations, were informed by the baseline boundary layer separation patterns.
Interestingly, the separation close to the root is also seen on the blade mounted with tubercles. However, the very first tubercle from left to right is seen to act as to prevent this separation to develop along the spanwise direction. The bubble is then limited to the narrow region downstream of the initial clean leading edge part of the blade.
Around mid-span and towards the blade tip, the paint indicates that the main effect provided by the tubercles on the blade surface develops close to the edges of the tubercles, as opposed to the tubercle centreline. The trends seen on other pitch and sweep angles are similar. However, care must be taken on the interpretation of these results. In the future, this qualitative analysis will be complemented by unsteady flow measurements immediately downstream of the blade trailing edge.

3.2 Aerodynamic Forces

Six components of force and moment data were obtained although only three main components are relevant (the axial force, F_x, the normal force, F_y, and the M_z moment). These were then used to obtain lift, drag, and pitching moment.

Aerodynamic coefficients and performance measured for clean and modified blades are illustrated in Fig. 7. Data at the five pitch angles studied are shown, and the sweep angle was fixed at $0°$. The baseline data is illustrated by red, cross markers. The other symbols represent tubercles along the full blade, from root to $2/3$ of the blade, and root region only ($1/3$ of the blade span).

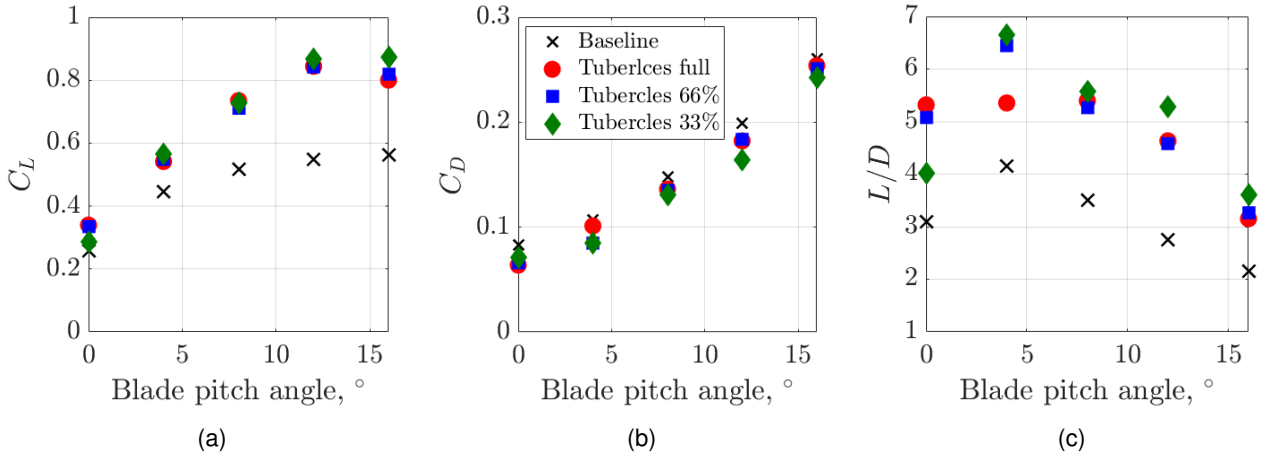

Figure 7 – Comparison of Lift and Drag Characteristics for the blade at zero sweep with and without full tubercles. U=36m/s (Rec = 1.44x105), sweep angle $0°$.

At zero sweep, the lift is augmented across the whole pitch range measured, where at the high pitch angles, the lift is almost doubled. At the same time the drag coefficient is seen to be marginally reduced, although the difference is on the same scale as the accuracy of the sensor used. The result is a significant improvement in lift to drag ratio of the unswept blade across the whole pitch range tested. Comparing the tubercles configurations, the denticles mounted close to the root display the best performance from pitch angle $4°$.
Results at $0°$ sweep, however, represent the best aerodynamic gains in terms of lift augmentation and L/D improvements for a large range of pitch angles. To illustrate this, Fig. 8 shows data for the same conditions presented in the previous figure, but for a $30°$ sweep angle. Data for the full tubercled blade configuration at $0°$ sweep is also displayed for reference (grey asterisks).

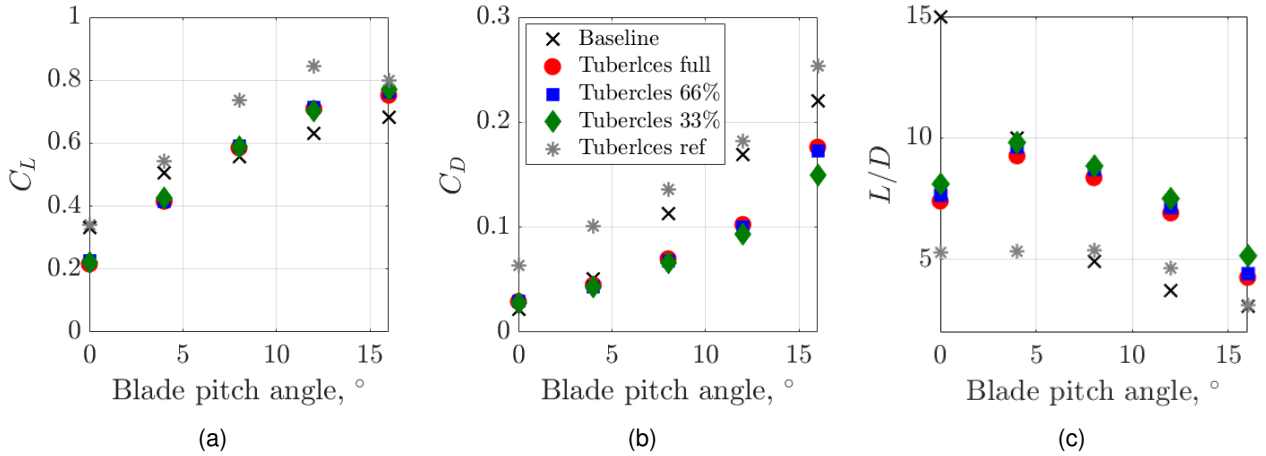

Figure 8 – Comparison of Lift and Drag Characteristics for the blade at zero sweep with and without full tubercles. U=36m/s (Rec = 1.44x105), sweep angle $30°$.

At higher sweep angles, although a striking reduction of the drag force is obtained, a reduction in lift at low to moderate pitch angles is also observed. The tubercles are seen to work well at high pitch angles. Thus, a substantial increment of the lift-to-drag ratio is seen from $8°$ pitch angle. This result

is important to the study in the next section, as the blade pitch angles studied in the propeller rig test are limited from 0 to 10°.
Overall, it has been observed that the tubercle flow control devices act to breakdown leading edge laminar flow, so the results for this previous experiment are likely to scale well with Reynolds number up to the scales involved in rotor rig testing. Although this is a very simplified experiment, both flow visualization and force data results are very encouraging. The next sections present sample data obtained from the new baseline propeller test rig.

4. Propeller Rig Baseline Results

Tests have been performed to validate the new installed propeller rig. The key results for forces, pressure distribution and vibration of the wing model are presented in this section.

4.1 Forces and Moments

Forces and moments measured for the propeller angular velocities, wind-speeds, blade angles and wing angles were recorded for the baseline blade configuration. Before further interrogating this data, the performance of the wing installed close to the propeller rig was evaluated. The propeller blades were removed for this experiment. Results are illustrated in Fig. 9.

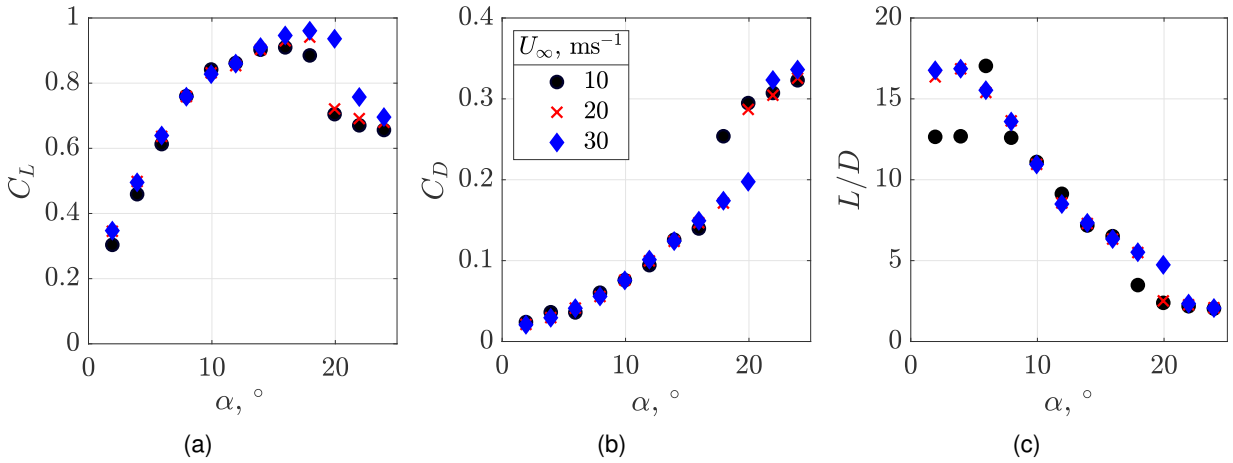

Figure 9 – Wing model C_L, C_D, and L/D measured at three wind-speeds.

Reynolds number effects acting on the wing are observed close to the stall angle. Based on the swept diameter, the Reynolds number varies from $0.5 < \mathrm{Re}/10^6 < 1.4$. Due to the resolution in angle of attack increments, it is difficult to establish the stall angle, but this value certainly increases with wind speed.
Based on the results for the isolated wing, the propeller tests focused on three wing angles, namely, 0°, 10°, 20°. Note that the last wing angle is clearly a stall condition for wind speeds 10 and 20 m/s, and just past stall for 30 m/s. The idea is to, in the future, run a complete investigation into whether the propeller wake, especially with tubercles mounted on the blades, is capable of delaying stall on the wing. Encouraging preliminary results are presented later in this work, in Sect. 5.

4.2 Pressure Distribution

Sample data for the pressure distribution measured for several propeller angular velocities is presented in Fig. 10. Based on the results presented in Fig. 9, stall has occurred in Fig. 10(b), but not in Fig. 10(a). The different combination of markers and colours represent data at five different propeller rotational speeds, including the wind-only configuration ($\mathrm{rpm} = 0$). The data was obtained on the mid-section of the wing (i.e., above the propeller tip).
At angle of attack equals to 10°, the propeller speed is seen to slightly increase the suction close to the leading edge, whilst decreasing the pressure along the lower surface of the wing. This is expected at these pressure taps span location, as the propeller increases the axial component of the

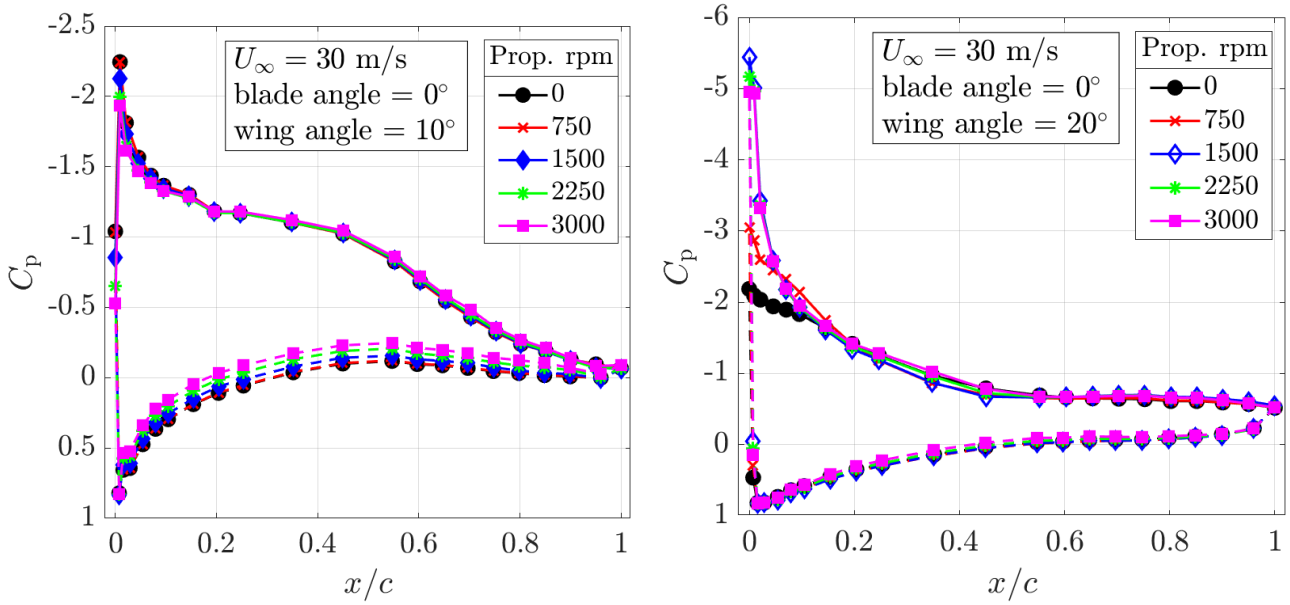

Figure 10 – Pressure coefficients measured for a range of propeller rpm. Wing angle (a) $10°$, and (b) $20°$

momentum on the lower surface, whilst decreasing the radial momentum on the upper surface of the wing (i.e., inducing flow away from the surface).

At $\alpha = 20°$, however, a much greater effect is seen on the suction side of the wing. The propeller slipstream strongly affects the pressure tap close to the wing trailing edge. The maximum suction is obtained for a rotational speed of 1500 rpm, indicating that the increased turbulence at higher rotational speeds limits the slipstream effect. Note that, at $U_\infty = 30$ m/s, the wing configuration is near the stalling angle.

It is important to stress that pressure taps were mounted along only two wing cross-sections and the aerodynamic coefficients are affected by a relatively large region in which the propeller wake interacts with the wing surface. Analysis of the pressure distribution results are carried out together with the vibration data, which is described in the next section.

4.3 Vibration Analysis

Preliminary tests demonstrated that the acceleration measured on the propeller is dominated by the motor operation. The data has given confidence in the hypothesis that the different pulley systems used to better control the speed of the propeller does not alter the rig vibration.

Acceleration measured on the wing has displayed clear contributions from the eigenfrequency of the wing structure and blade passing frequencies. An example is shown in Fig. 11. This figure also indicates the background noise of the accelerometer signal (dashed grey line). Results are also consistent in wind-on experiments (Fig. 11(b)).

The eigenfrequency of the wing model structure and the blade pass frequency are clearly dominant at 3000 rpm. As expected, increase in wind speed favours the eigenfrequency whilst reducing the motor rotation frequencies and blade pass frequency. Lower propeller rotational speeds will have less influence on the wing vibration, so additional care must be taken to analyse those results.

The amplitude of the blade passing frequencies are also a function of the blade pitch angle and, to a lower extent, the wing angle of attack. The authours intend to study these relationships in the near future, but the main focus of the present paper is on the comparison between clean blades and blades with tubercles. This investigation is presented in the next section.

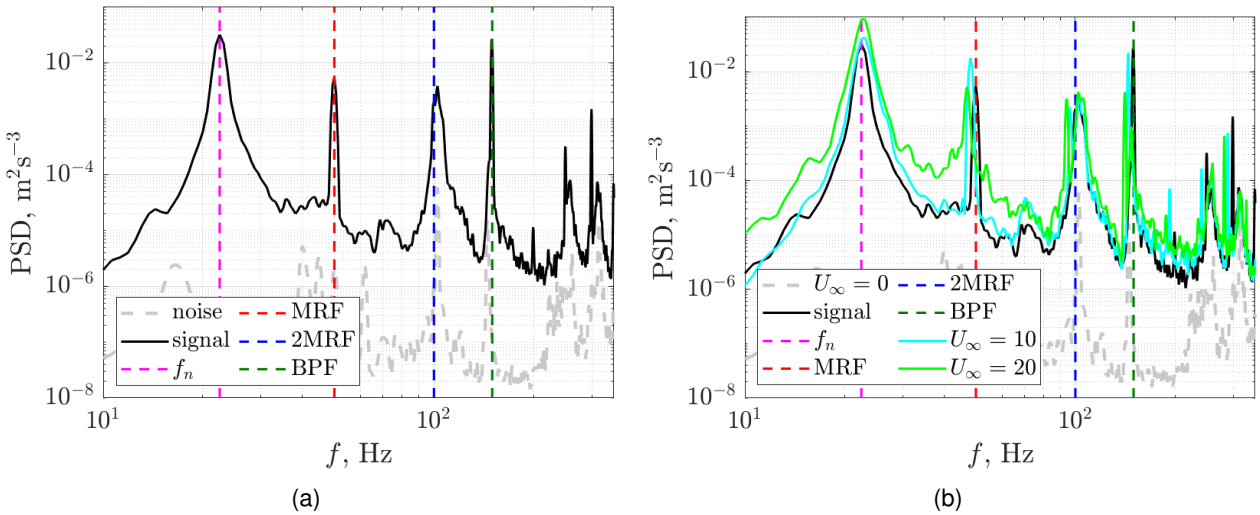

Figure 11 – PSD of the acceleration measured on the wing. (a) no-wind test; (b) no-wind and two wind-on tests. The propeller rotational speed in both graphs is 3000 rpm

5. Effect of Tubercles

5.1 Aerodynamic forces

The final campaign described in Section 2.4has been carried out and preliminary analysis of the data is described in this section. The first study conducted regards changes in wing performance with propeller rotational speed and presence of the tubercles along the blade leading edge.

Figure 12 displays aerodynamic coefficients and lift-to-drag ratio of the wing model at $U_\infty = 20$ m/s and $\beta = 5°$. Data for the isolated wing configuration is illustrated by cross markers. The other two set of markers represent data obtained for a propeller rotational speed of 3000 rpm, with tubercles (blue dots) and without tubercles (red circles) mounted along each of the three propeller blades.

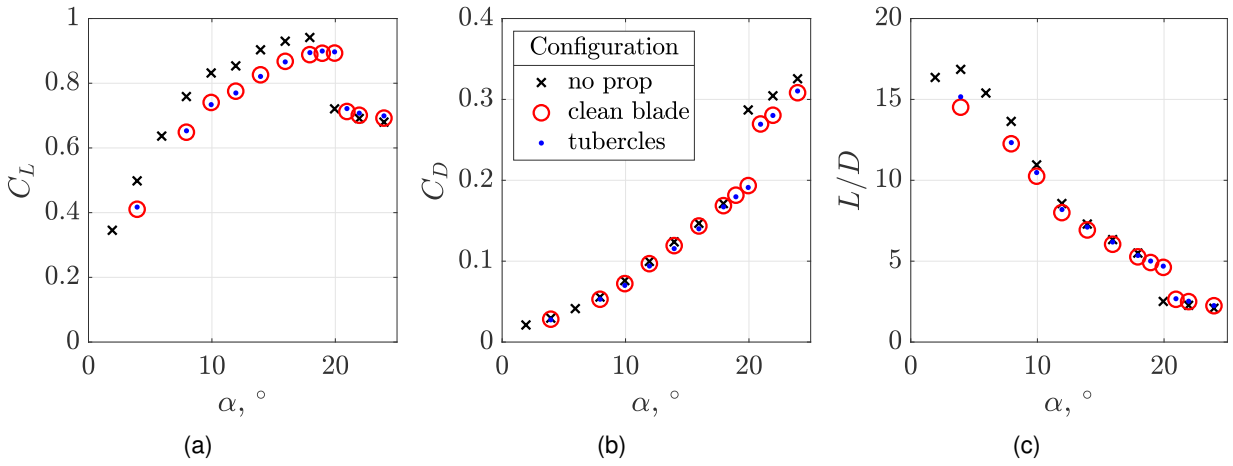

Figure 12 – Wing model C_L, C_D, and L/D obtained with no propeller (x markers), propeller with clean blades (circles) and blades with tubercles (dots). Wind speed equals to 20 m/s and propeller rotational speed 3000 rpm. Blade pitch angle 5°.

Two main trends regarding the aerodynamic coefficients are observed. Firstly, although no significant changes are seen for the drag force, the lift coefficients reduce slightly when the propeller wake interacts with the wing. Secondly, the propeller wake delays stall in comparison with the isolated wing configuration. These results translate into a lower efficiency of the wing at angles of attack $\alpha \leq 12°$, whilst only a marginal difference is seen at higher angles.

Regarding the effect of tubercles, a slight improvement on the lift-to-drag ratio is observed for most angles of attack. The circle and dot markers were chosen to illustrate this difference, which is smaller

than the delta between wing only and propeller-wing test conditions. Repeat tests have been conducted and display similar results. Errors and relative uncertainty of the current measurements are being computed and will be made available in Cranfield's MENtOR final report.

5.2 Pressure distribution

Similarly to the commissioning tests, the pressure distribution along two wing cross-sections has been studied. Figure 13 illustrates pressure distributions of a clean blade propeller configuration and a full tubercle blade case, both at a blade pitch angle of $5°$. A third dataset has been included, which corresponds to the tubercle blade at $\beta = 0°$ test. Additional nominal test conditions are described on figure caption.

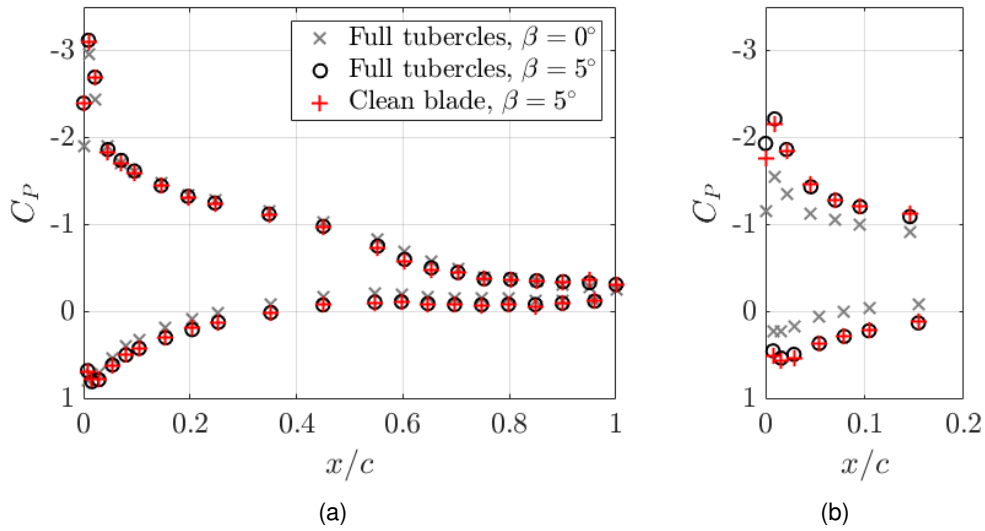

Figure 13 – Pressure distribution along the cross-sections located at (a) 0.50 m above the propeller axis and (b) 0.15 m above the propeller axis. Wing angle of attack at $16°$; wind speed 20 m/s; 3000 rpm; and blade pitch angle $0°$ and $5°$

Above the propeller tip (Fig. 13(a)), no significant difference is observed between the clean blade and tubercles blade at equivalent blade pitch angle. This result has also a weak dependence on blade pitch angle, although a small difference is seen along both the suction and pressure sides.
Close to the root of the propeller, the pressure distribution on the wing depends more strongly on the propeller blade properties. This agrees with the peak on additional loading provided by the propeller slipstream [6]. Tubercles will provide a minor effect close to the leading edge and the blade pitch angle clearly affects the results presented in Fig. 13(b).
Finally, to illustrate data at post-stall angle of attack, Fig. 14 displays the pressure distribution for clean and tubercles blade at $\alpha = 20°$. The blade pitch angle for all curves is $\beta = 10°$, all other properties are replicated from Fig. 13.
As expected, no significant difference is seen between the baseline and the blade with tubercles in Fig. 14(a). The pressure distribution clearly indicates stall over the wing. In Fig. 14(b), the propeller wake affects both the upper and lower surfaces of the wing. The tubercles produce a more distinguished effect in comparison to what was observed at $\alpha = 16°$.
In summary, the pressure distribution data is in agreement with the global force measurements on the wing. The main differences between the clean blade baseline and the blade mounted with tubercles are confined to the region close to the propeller root and nacelle. The propeller slipstream, which is independent of the tubercle configurations studied, drive the main differences seen in the wing performance.

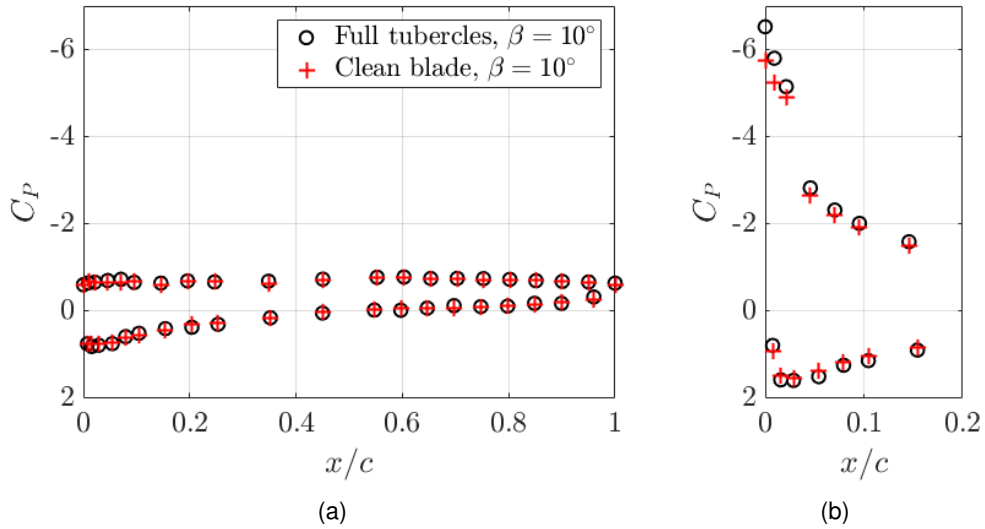

Figure 14 – Pressure distribution along the cross-sections located at (a) 0.50 m above the propeller axis and (b) 0.15 m above the propeller axis. Wing angle of attack at $20°$; wind speed 20 m/s; 3000 rpm; and blade pitch angle $10°$.

5.3 Vibration

To complete this preliminary analysis, data from the accelerometer mounted on the wing has been analysed. A sample result is displayed in Fig. 15, which displays the power spectral density for clean blades and blades with tubercles.

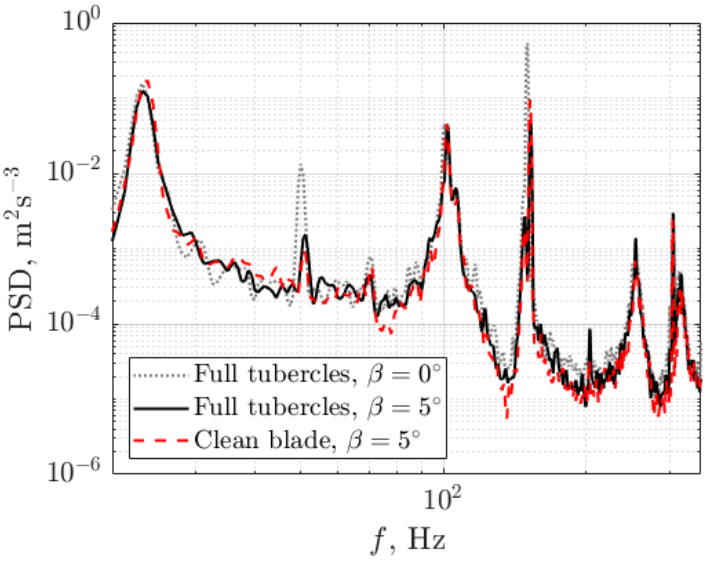

Figure 15 – Power spectral density of the acceleration measured on the wing at $U_\infty = 20$ m/s, angle of attack $16°$, and propeller rotational speed 3000 rpm. Data for clean blade and two full tubercles blade angles are shown.

In line with results presented in the previous two sub-sections, the tubercles have not provided substantial changes to the vibration modes of the wing. The amplitude and location of the wing model eigenfrequency, motor rotation and blade passing frequency from clean blade (dashed, red line) and blade with tubercles (solid, black line). Note the tubercle data for a different blade pitch angle has also been added for reference (dashed grey line). The accelerometer data stresses once more that the differences seen are due to the changes in the propeller wake caused by different blade configurations, rather than the presence of the denticles.

6. Conclusions

This paper presented an experimental investigation into a small-scale propeller rig to study installed propeller flows. The design of the propeller blades was conducted in collaboration with MENtOR project partners. An isolated static blade was investigated before manufacturing the three-blade propeller rig and vortex generators to be mounted along the leading edge of the blades. Results from the static blade experiment suggest that these tubercle-shaped devices substantially increase the normal force acting on the propeller blades. Flow visualization tests suggest that the separation regions observed near the trailing edge of the clean blade are reduced due to the presence of the tubercles.

The propeller rig was then manufactured and commissioned over two test expeditions conducted in the 8x6 Wind Tunnel, at Cranfield University. The first campaign focused on investigating the propeller rig capabilities under wind speeds up to 30 m/s, propeller rotational speed up to 3000 rpm, and pitch blade angle up to 10°. The wing mounted downstream of the propeller plane was investigated from 0° to 22°. In the present work, instead of focusing on tilting manoeuvres, the angle of attack was set to investigate the effect of slipstream on the wing efficiency.

The commissioning campaign was performed successfully. Measurements on the wing indicate that 1) the propeller slipstream delays stall, but decreases lift and lift-to-drag ratio at angles of attack lower than 12°, 2) the pressure distribution is altered significantly due to the propeller wake, and this effect increases with blade pitch angle, 3) after stall, the pressure distribution is significantly affected by the propeller wake only close to the blade root, and 4) the accelerometers mounted on the wing correctly capture the blade passing frequency and its harmonics.

Preliminary results obtained from the second campaign were also included in the paper. The benefits of mounting tubercles observed in the static test were not seen in the propeller rig data. Only a slight increase in the lift-to-drag ratio was obtained and at low angles of attack. Wing stall was apparently unaltered by the tubercles. The pressure distribution along the suction side of the wing is improved, but only at locations close to the propeller nacelle. A similar result was observed on the anemometer data, where the amplitude of the dominant frequencies are seen to be a function of blade pitch angle, but not blade configuration.

Nonetheless, the data acquired in the tests described in the paper will be assessed fully before the next campaign is performed. Firstly, the experimental relative uncertainty is being computed. This analysis together with the results obtained for all test runs will be made available at Cranfield Online Research Data (CORD) research repository. Additionally, the rig is currently being redesigned to measure propeller thrust and torque. Finally, the propeller flow field will be investigated in a dedicated particle image velocimetry experiment.

Contact Author Email Address

mailto: a.proenca@cranfield.ac.uk

Acknowledgments

The authors would like to thank the AAL technicians involved in this work. Lynton Banks-Davies and Karl Gerhard were responsible for setting up and assisting with the experiments. Paul Dancer designed and built both the static blade and the propeller test rigs. Research assistant Estela Bragado Aldana provided pivotal assistance to the final test programme. Previously a research fellow within the AAL group, Francesco Dorigatti is acknowledged for several contributions in the early stages of this research. This work is supported by the EPSRC project MENtOR: Methods and Experiments for NOvel Rotorcraft (EP/S013814/1).

Copyright Statement

References

[1] Seddon, J M and Newman, S. *Basic Helicopter Aerodynamics*. 3rd edition, Aerospace Series, Wiley, 2011.

[2] Ribner, H S. Notes on the Propeller and Slipstream in Relation to Stability. *NACA Wartime Report*, 1944.

[3] Kroo, I. Propeller-wing integration for minimum induced loss. *Journal of Aircraft*, Jul;23(7):561-5, 1986.

[4] Witkowski, D, Johnston, R and Sullivan, J. Propeller/wing interaction. *In 27th Aerospace Sciences Meeting*, 1989.

[5] Fratello, G, Favier, D and Maresca, C. Experimental and numerical study of the propeller/fixed wing interaction. *Journal of Aircraft* 28:6, 365-373, 1991.

[6] Veldhuis, L L. Review of propeller-wing aerodynamic interference. *In 24th International Congress of the Aeronautical Sciences*,Vol. 6, No. 1, 2004.

[7] Chauhan S S and Martins J R. Rans-based aerodynamic shape optimization of a wing considering propeller–wing interaction. *Journal of Aircraft*, 58(3):497-513, 2021.

[8] Sinnige, T, van Arnhem, N, Stokkermans, T C A, Eitelberg, G and Veldhuis, L L M. Wingtip-Mounted Propellers: Aerodynamic Analysis of Interaction Effects and Comparison with Conventional Layout. *Journal of Aircraft*, 56, 1, 2019.

[9] Butt, F R and Talha, T. Numerical Investigation of the Effect of Leading-Edge Tubercles on Propeller Performance. *Journal of Aircraft* 56:3, 1014-1028, 2019

[10] Gruber, T, Murray, M and Fredriksson, D. Effect of Humpback Whale Inspired Tubercles on Marine Tidal Turbine Blades. *ASME 2011 International Mechanical Engineering Congress and Exposition*, 2011

[11] Zhao, M, Xu, L, Tang, Z, Zhang, X, Zhao, B, Liu, Z and Wei, Z. Onset of dynamic stall of tubercled wings. *Physics of Fluids*, 33, 081909, 2021.

2022-11-28

Experimental evaluation of a passive flow-control device for a tiltrotor aircraft

Proenca, Anderson R.

Proenca AR, Prince SA, Banks-Davies L, Garry KP. (2022) Experimental evaluation of a passive flow-control device for a tiltrotor aircraft. In: ICAS 2022: 33rd Congress of the International Council of the Aeronautical Sciences, 4-9 September 2022, Stockholm, Sweden
https://www.icas.org/ICAS_ARCHIVE/ICAS2022/data/preview/ICAS2022_0530.htm